

No-Reference Image Quality Assessment Based on Natural Scene Statistics in NSCT Domain and Spatial Domain

GUIYING ZHU

*Department of Applied Engineering
Zhejiang Institute of Economics and Trade
Hangzhou, Zhejiang, 310018 P.R. China*

E-mail: zhuguiyingdn@163.com; guiying_zhu12@aol.com

No-reference / blind image quality assessment (NR-IQA) methods aim to predict the quality of distorted images with respect to human perception automatically without prior knowledge of reference images. We present an efficient general-purpose NR-IQA method in this research using natural scene statistics (NSS) in nonsubsampling contourlet transform (NSCT) domain and spatial domain, which we name TDSDQA. Firstly, we analyze the strong correlation of parent-child coefficients and relative coefficients in NSCT domain, and calculate the mutual information (MI) between those coefficients to describe their correlation. Second, the structure similarity of those coefficients is determined and utilised to represent the picture structure information statistics. In addition, when used in conjunction with the arithmetic perfect of close by normalised brightness constants in the three-dimensional area, we extract 84 statistics features which are sensitive to the presence and severity of image distortion. At last, these features are used to predict image quality scores in a support vector regression (SVR) approach, and the assessment approach is tested on LIVE and TID2008 IQA database. The experimental results show that this method is suitable for many common image distortion types and correlates well with the human judgments of image quality. And that, it has highly competitive performance to other state-of-the-art NR-IQA algorithms in many respects, such as database independence, classification accuracy, computational complexity and so on.

Keywords: no-reference/blind image quality assessment, natural scene statistics, nonsubsampling contourlet transform, mutual information, support vector regression (SVR)

1. INTRODUCTION

In recent years, there has been a surge in interest and demand for accurate, user-friendly, and practical image and video quality assessment (IQA) and video quality assessment (VQA) tools that a number of practical multimedia signal acquisition applications, it may be used to analyse, regulate, and improve the perceived quality of multimedia material. [24] communication, and display systems [1]. For image quality standards, the quality of digital photographs is determined by a number of factors. The major criteria of image quality include resolution, noise, and artefacts. The use of computer models to forecast video quality in accordance the human visual system's perception is known as objective video quality assessment (VQA) (HVS). No-reference (NR)/blind approaches [2-8] in which the algorithm is only given the distorted stimulus are those that are subjected to quality evaluation. The importance of NR image quality measurements is mostly due to two factors. On the one hand, NR image quality measurements are useful in applications where obtaining a reference picture is difficult or impossible. On the other hand, the fact that the human visual

system (HVS) can quickly assess picture quality without any prior knowledge drives the NR-IQA study. The eye, the adjacent geniculate nucleus (LGN), and the visual cortex – the region of the brain that interprets visual information – make up the human visual system (HVS).

Researchers think that the HVS evolved as a result of visual stimuli from the natural world, and thus modelling real situations and the HVS are fundamentally two separate challenges [23]. Moreover, Natural images meet some distribution rules and the statistical properties of natural scene are consistent with the perception characteristics of HVS. As a result, the essential characteristics are either identified or described utilizing NSS. NSS methods are based on the concept that pictures of the natural world (*i.e.*, distortion-free images) inhabit a limited subspace of the total space of all conceivable images, and strive to discover a distance between the test image and this subspace [9]. The basic observation of the approaches is that real photographs have certain statistical properties that may be expressed by a mathematical model and are distorted by a number of factors. Nowadays, most of the NSS approaches can be broadly classified as spatial domain and transform domain.

Three-dimensional NSS prototypical does not need a plotting to a dissimilar co-ordinate area (DCT, ripple, contourlet, NSCT, *etc.*). The new approach, named BRISQUE relies on scene statistics of regionally normalized brightness coefficients rather than distortion-specific features like ringing, blur, or blocking to determine distortion-specific characteristics like ringing, blur, and blocking to evaluate putative image “naturalness” losses. In [10, 11], the authors proposed The BRISQUE technique combines scene statistics of regionally normalized brightness coefficients to assess any losses of “naturalness” in the image caused by distortions, resulting in a holistic assessment of quality. Natural scene statistics (NSS) is a frequently used NR IQA measure that believes natural pictures have certain regular statistical features. The basic elements of an empirical distribution of locally normalized luminance and their products is used to create a spatial natural scene statistic model. Liu [12] utilized entropies calculated from resident picture chunks, for together chunk three-dimensional measure replies and block DCT coefficients, the DC coefficient, or average sample value, is the DCT coefficient (0,0). Low frequency coefficients are often greater values, whereas high frequency coefficients are typically smaller values, since real pictures fluctuate very minimally from sample to sample. After that, the system generates a 12-dimensional local entropy feature vector from which it learns to predict image quality scores. The authors in [13] used self-correlated mutual information as features to quantify the correlations between neighboring pixels of original natural images and their corresponding normalized luminance field and local standard deviation field. Mutual information is one of several terms that describe how much information one random variable may provide about another. Spatial NSS model is “transform-free” and highly efficient.

In [14], the authors extracted the features were created using an NSS model of the picture DCT coefficients and the model’s estimated parameters to create perceptual quality characteristics. Then, using a basic Bayesian inference technique, these traits were utilized to predict quality ratings. In [15], Mittal *et al.* extracted 88 statistical features in DWT domain based on the no-reference image quality assessment model. There are high relationships between geographically co-located/neighboring coefficients from different scales and orientations, and then used a two-stage blind IQA framework that first identifies the image distortion and then performs distortion-specific quality evaluation. On this basis, [16] applied the complex generalized Gaussian supply, The usual distribution, also known as the Gaussian distribution, is a balanced possibility circulation positioned on the unkind,

representative that information everywhere the unkind happen more often than information distant from it, generalized Gaussian distribution [22] and the wrapped Cauchy distribution to model wavelet coefficient magnitudes, wavelet coefficients' relative magnitudes and those relative phases respectively, and then used to quantify the deterioration of relationships across picture scales, use the complex wavelet structural similarity index. The organizes of the highest of the log-histograms of the curvelet constants standards, as well as the vigor deliveries of together positioning and gage in the curvelet area, were retrieved by Liu *et al.* in [17]. to assessment image quality. In [18], The authors recommended predicting the natural tendency of additional susceptible parts in the shearlet domain using the most natural parts of an image and comparing the projected portions to the real inaccurate sections using the most natural parts of an image. In [19], the authors studied the NSS of the transformation coefficients in the transformed space and thought. On peak coordinate space, the peak coordinates of the modified coefficient histogram of filtered natural pictures create well-defined clusters, and then obtained a reliable statistical relation between the image quality levels and ICs Using a combination of curvelet, wavelet, and cosine transforms.

While the above-mentioned methods Each of them has specific restrictions when it comes to delivering excellent NR-IQA results. BLINDS-II [14], DIIVINE [15] and C-DIIVINE [16] are difficult to compute in real time. Although SSEQ [12], MIQA [13] and CurveletQA [17] are more efficient, across all distortion categories, they don't fare well in terms of association with human perception. In BRISUE [11], MSCN coefficient distribution of different natural undistorted image may have obvious difference, but that of different distorted versions and different distorted degree images may have similar or identical distribution. In these circumstances, it fails to correctly assess images quality and is also unable to correctly identify their distortion types. In order to get an available, well-performed and robust NR-IQA based on NSS, we discovered that image when distorted can affect the strong correlation and the structural information between its NSCT coefficients. Motivated by this, we suggest a well-organized all-purpose NR-IQA algorithm using NSS in NSCT domain and spatial domain. In addition, in order to analyze the correlation with human opinions, the database independence, the classification accuracy and the computational complexity, a huge amount of imitation tests are carried out in the LIVE [20] and TID2008[21] IQA record. The simulation results suggest that this approach can handle a wide range of distortions and consistent with subjective assessment, and the Spearman's Rank Ordered Correlation Coefficient (SROCC) and the Pearson's Linear Correlation Coefficient (PLCC) are two types of correlation coefficients. (PLCC) in LIVE IQA database are more than 0.95. The Spearman rank-order correlation coefficient (also known as Spearman's correlation) is a nonparametric measure of the strength and direction of relationship between two variables assessed on an ordinal scale. Pearson's Linear Correlation Coefficient provides information on the degree and direction of a relationship's linkage, or correlation. And the recognition accuracy of the recognition model is up to 94.23% and significantly superior to all distortion-generic NR-IQA in use today.

2. THE ANALYSIS OF STATISTICAL FREATURES OF MSCN COEFFICIENTS

Ruderman [22] advocated using local mean subtraction and divisive normalization to

generate locally normalized luminance. He then performed a resident non-linear process on log-contrast brightness's to normalize the local variance of the log contrast and decrease resident mean movements from null log-contrast. The mean subtracted contrast normalized (MSCN) coefficients can be used to mimic the contrast-gain masking process in early human vision, according to A. Mittal [11]. Analyse the distribution of Mean-Subtracted Contrast-Normalized (MSCN) coefficients on local spatial neighbourhoods of a given picture. It is well known that such a distribution acts naturally for natural pictures, although distortions of various types disturb this regularity.

Given $I(i, j)$ is an $M \times N$ intensity duplicate, its MSCN constants can be produced:

$$\hat{I}(i, j) = \frac{I(i, j) - \mu(i, j)}{\sigma(i, j) + C}. \quad (1)$$

Where, $\mu(i, j) = \sum_{k=-K}^K \sum_{l=-L}^L \omega_{k,l} I_{k,l}(i, j)$, $\sigma(i, j) = \sqrt{\sum_{k=-K}^K \sum_{l=-L}^L \omega_{k,l} (I_{k,l}(i, j) - \mu(i, j))^2}$, $i = 1, 2, \dots, M$, $j = 1, 2, N$; $C = 1$ is the denominator approaches 0, this constant prevents instability when an image patch corresponding to the plain sky.

$\omega = \{\omega_{k,l} | k = -K, \dots, K; l = -L, \dots, L\}$ is a circularly symmetric Gaussian weighting function in two dimensions that has been sampled to rescaled to unit volume and three standard deviations.

Ruderman also believed that for nature photographs, these normalized brightness values strongly tended towards a unit normal Gaussian characteristic. As a result, a generalized Gaussian delivery (GGD) might be employed to arrest a larger range of picture statistics. The GGD is

$$f(x; \alpha, \sigma^2) = \frac{\alpha}{2\beta\Gamma(1/\alpha)} \exp(-(|x|/\beta)^\alpha). \quad (2)$$

Where, $\beta = \sigma \sqrt{\Gamma(1/\alpha) / \Gamma(3/\alpha)}$, $\Gamma(x) = \int_0^\infty e^{-t} t^{x-2} dt (x > 0)$ is the spectrum purpose. The shape constraint determines the variance as well as the form of the distribution.

A. Mittal then used empirical distributions of surrounding MSCN coefficients to simulate statistical correlations between neighbouring pixels along horizontal, vertical, main-diagonal, and secondary-diagonal orientations, as shown in Fig. 1. And he reasoned that the asymmetric generalized Gaussian distribution (AGGD) model may be a reasonable

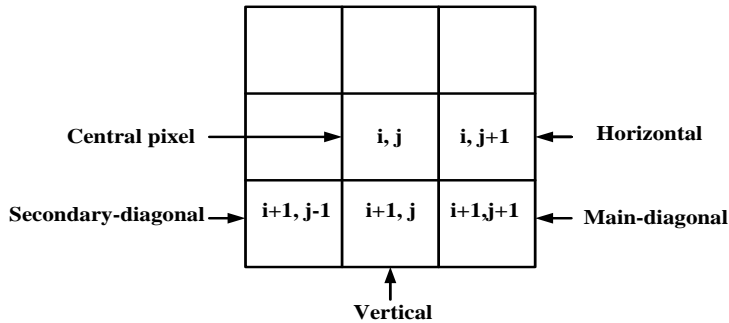


Fig. 1. Contiguous MSCN coefficients in horizontal, vertical, main-diagonal, and secondary-diagonal orientations.

match to the actual histograms of those nearby coefficients as a practical alternative. On the real line, the asymmetric generalized Gaussian distribution (AGGD) belongs to one of two families of parametric continuous probability distributions. The normal distribution is given a shape parameter in both families.

The neighboring MSCN coefficients can be produced:

$$\begin{cases} H(i, j) = \hat{I}(i, j)\hat{I}(i, j+1) \\ V(i, j) = \hat{I}(i, j)\hat{I}(i+1, j) \\ D_1(i, j) = \hat{I}(i, j)\hat{I}(i+1, j+1) \\ D_2(i, j) = \hat{I}(i, j)\hat{I}(i+1, j-1) \end{cases} \quad (3)$$

The AGGD with zero mode is given by:

$$f(x, \alpha, \sigma_l^2, \sigma_r^2) = \begin{cases} \frac{\alpha}{(\beta_l + \beta_r)\Gamma(1/\alpha)} \exp(-(-x/\beta_l)^\alpha) & x < 0 \\ \frac{\alpha}{(\beta_l + \beta_r)\Gamma(1/\alpha)} \exp(-(-x/\beta_r)^\alpha) & x \geq 0 \end{cases} \quad (4)$$

Where, $\beta_l = \sigma_l \sqrt{\Gamma(1/\nu)/\Gamma(3/\nu)}$, $\beta_r = \sigma_r \sqrt{\Gamma(1/\nu)/\Gamma(3/\nu)}$. The shape parameter ν controls the shape of distribution and the scale parameters σ_l^2 , σ_r^2 control the spread on each side of the mode respectively.

The MSCN coefficients and their neighboring coefficients have characteristic statistical properties that are changed by the presence of distortion so the parameters (α, σ^2) of GGD fitted the empirical distribution of MSCN coefficients and the parameters $(\eta, \alpha, \sigma_l^2, \sigma_r^2)$ ($\eta = (\beta_r - \beta_l)\Gamma(2/\alpha)/\Gamma(1/\alpha)$) of AGGD fitted the empirical distribution of neighboring MSCN coefficients can be used to capture image distortion as statistic features in spatial domain. Images are naturally multiscale and distortions affect image structure across scales. Increasing the number of scales beyond two did not improve performance considerably, according to research [11] so we cutting all MSCN statistic structures at the creative copy scale and a reduced resolution in this paper. There are an entire of 36 structures-18 features at each scale in spatial domain.

One of the publicly available picture quality databases is LIVE, which was established at the University of Texas in Austin. In 24-bpp colour BMP format, it comprises 29 reference photos and 779 distorted images. Jpeg2000 compression (jp2k), jpeg compression (jpeg), Additive gaussian white noise (wn), Gaussian blurring (gblur), and jpeg2000 with bit errors through a simulated Rayleigh fading channel are the five distortion kinds in this database (ff). Rayleigh fading is a statistical model that describes how the propagation environment affects a radio signal, such as that used by wireless devices. In the study of images from the LIVE IQA database, we find that MSCN coefficient distribution of different natural undistorted image may have obvious difference, such as image “buildings” and “plane” *etc*. The parameters (α, σ^2) of GGD model fitted the empirical distribution of their MSCN coefficients are shown in Table 1. In addition, the MSCN coefficient distribution of different distorted versions and different distorted degree images may have similar or identical distribution, such as natural undistorted image “cemetery” and jpeg distorted

image “dancers” *etc.* The parameters (α , σ^2) of GGD model fitted the empirical distribution of their MSCN coefficients, their distorted versions and DMOS are shown in Table 2. The situation is similar in other IQA database, like TID2008 and CSIQ [23] *etc.*

Table 1. Part of natural undistorted images from the live IQA database whose MSCN coefficients distribution has the obvious difference.

image	GGD model fitted the distribution of MSCN coefficients	
	shape parameter α	Standard deviation σ
“buildings”	3.3080	0.4087
“plane”	1.1410	0.2301
“carnivaldolls”	1.5290	0.2371

Table 2. Part of different distorted versions and different distorted degree images from the live IQA database whose MSCN coefficients distribution are similar or identical.

image	Distorted type	DMOS	GGD model fitted the distribution of MSCN coefficients	
			shape parameter α	Standard deviation σ
“cemetery”		0	2.4360	0.3647
“dancers”	natural undistorted jpeg	26.8204	2.4350	0.3678
“carnivaldolls”		0	1.5290	0.2371
“ocean”	natural undistorted jpeg	22.4278	1.5300	0.2419
“manfishing”		0	2.1060	0.3247
“cemetery”	natural undistorted jp2k	31.3871	2.1100	0.3273
“rapids”	natural undistorted	0	2.5720	0.3518
“caps”	ff	21.1665	2.5710	0.3601
“churchandcapitol”	natural undistorted	0	2.0530	0.2919
“buildings”	ff	44.8420	2.0530	0.2996
“plane”	jp2k	25.9840	1.8290	0.2788
“lighthouse2”	jpeg	41.5000	1.8330	0.2784
“house”	jpeg	58.7879	0.8330	0.1882
“plane”	ff	24.7848	0.8330	0.1920

In these circumstances, the statistical features advanced by A. Mittal fail to correctly assess these images quality and are also unable to correctly identify their distortion types. However, the correlation between NSCT subband coefficients of these images may be different. One of the new geometrical image transforms is the nonsubsampled contourlet transform (NSCT). To create a multiscale and multidirectional decomposition of a picture, this transform employs nonsubsampled pyramids (NSP) and nonsubsampled directional filter banks (NSDFB). Driven by this, we present a general-purpose NR-IQA method using NSS in NSCT domain and spatial domain.

3. NSCT AND THE RELATIONSHIP BETWEEN ITS COEFFICIENTS

3.1 NSCT

Some efficient multiscale image representation, such as the Gabor, the wavelets and the contourlet transforms, have the ability to capture significant information of an object

of interest given a small description. For picture representations, is a novel two-dimensional transform technique. The contourlet transform may effectively capture it with only a few coefficients. They are also at the heart of a lot of image processing jobs, such compression and denosing. Da Cunha [24] presented a shift-invariant version of CT, dubbed NSCT, to eliminate the contourlet transform’s frequency aliasing and improve its directional selectivity and shift-invariance. The nonsubsampling pyramid (NSP) achieves the NSCT’s multiscale capability by splitting the frequency plane into a low-frequency subband and multiple annular high-frequency subbands using nonsubsampling filters (NSFs). When compared to the contourlet transform, we use the NSF’s less rigorous design constraint to create filters that result in an NSCT with greater frequency selectivity and regularity. A directional filter that is not subsampled. The nonsubsampling directional filter bank’s bank idealized frequency response is known as NSDF. Meanwhile, nonsubsampling directional filters (NSDFs) gain the multi-directional feature by further integrating high-frequency coefficients into wedge-shaped directional subbands. The NSCT is a completely shift-invariant, multi-scale, multi-direction expansion with improved directional frequency localization and a short implementation time.

Fig. 2 (a) depicts an overview of the NSCT, whereas Fig. 2 (b) depicts the frequency division of the nonsubsampling contourlet decomposition, in which the entire spectrum is divided both angularly and radially, with the number of directions increasing as frequency increases. In essence, the NSCT structure provides a subband decomposition comparable to that of contourlets, but without the need of downsamplers and upsamplers.

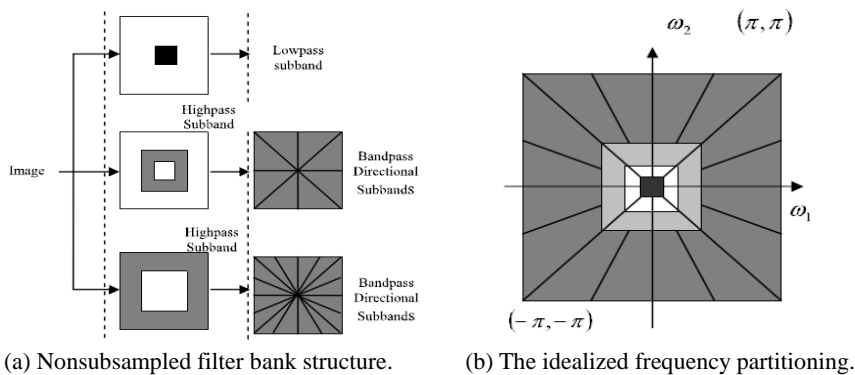


Fig. 2. The nonsubsampling contourlet transform.

3.2 The Relationship Between NSCT Coefficients

Performing NSCT on one image can be obtained one low-frequency and a series of high-frequency sub-images which have the same size as the source image at each level and direction. On the one hand, those high-frequency sub-images have independent distributions with a high peak at zero amplitude and long tails on both sides (the phenomenon is called heavy-tail) respectively. On the other hand, there exists correlation between them. In order to visualize some important correlation between those high-frequency sub-images, Fig. 3 visually displays some of these correlations for a single picture split into two layers with four and eight orientations, respectively.

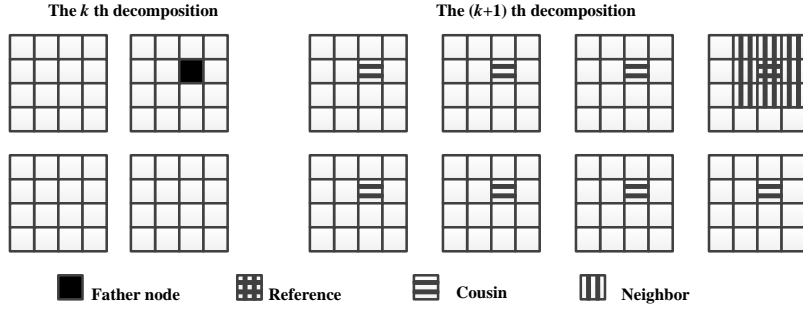


Fig. 3. The relationship of NSCT coefficients.

We define the eight neighbouring NSCT coefficients in the same subband as their neighbours for each NSCT coefficient (c). Then, in the immediately coarser scale, the coefficients in the same spatial region correspond to its parent (c), and in the immediately finer scale, the coefficients in the same geographic location correspond to its child coefficients. Each coefficient has one parent and eight children to consider. Apart from the cross-scale and intra-subband relationships, cousins (c) relate to coefficients in the same scale and geographical location but in distinct directional subbands.

In order to describe the correlation between different NSCT subband coefficients, we use the correlation coefficients (CC). Suppose X and Y are two different NSCT subband coefficients of the same image, the CC between them is given by:

$$r = \frac{\sum_i^M \sum_j^N (X_{ij} - \bar{X})(Y_{ij} - \bar{Y})}{\sqrt{\sum_i^M \sum_j^N (X_{ij} - \bar{X})^2 \sum_i^M \sum_j^N (Y_{ij} - \bar{Y})^2}} \quad (5)$$

Where \bar{X} , \bar{Y} are the mean of X , Y respectively, and $-1 \leq r \leq 1$.

Fig. 4 shows box plot of the mean CC between parent-child coefficients, relative coefficients which are a coefficient and its cousins or other coefficients for natural undistorted images from the LIVE IQA database. From Fig. 4, we can see that the correlation between relative coefficients is the strongest and the correlation between other coefficients is the weakest.

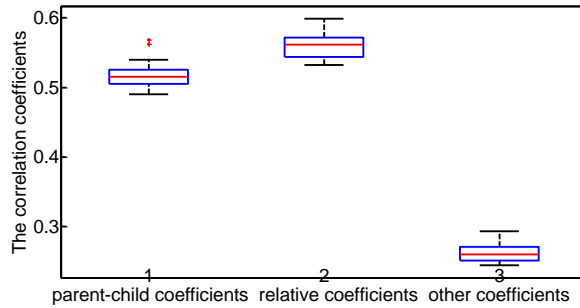


Fig. 4. The correlation coefficients between NSCT subbands.

3.3 The Influence of Various Distorted Versions to the Relationship Between NSCT Coefficients

Image distorted will change the distribution of information, and the effects of different distortion types and degrees are also different. In NSCT domain, the high-frequency sub-band coefficients must change and it also will lead to the correlation between them vary. In order to visualize how the correlation between different NSCT subband coefficients varying, using the LIVE IQA database, Fig. 5 depicts the mean CC between those coefficients for all natural undistorted pictures and their different distorted variants. Figure 5 shows that distortion-specific clustering is seen regardless of content, and that various distortions occupy distinct sections of the space. As a result, we believe that the existence of distortion alters the correlation statistical features of NSCT subband coefficients, and that measuring these changes will allow us to forecast the type of distortion impacting a picture as well as its perceived quality.

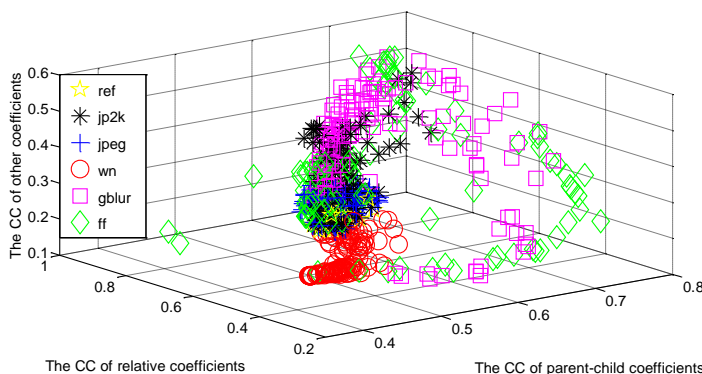


Fig. 5. From the LIVE IQA database, the CC between NSCT subbands for normal, undistorted pictures and their numerous warped variants.

4. THE NR-IQA MODEL IN NSCT DOMAIN AND SPATIAL DOMAIN

4.1 The Mutual Information

MI of two random variables can assess mutual dependency on the variables or how much one random variable informs us about another in probability and information theory. It's a dimensionless number using bits as units, and it's defined as the reduction in uncertainty about one random variable when another is known. In the field of image processing, the MI is correlation measure based on the gray value statistics of the image. It is not directly dependent on the gray value of the image, but measures the relationship between different image according to the relative probability of the gray values in each image and the joint probability within the overlap region of the 2 pictures.

Suppose X and Y are two different images of the same size, and MI between X and Y can be defined as:

$$MI(X, Y) = \sum_{y \in Y} \sum_{x \in X} p_{XY}(x, y) \log \left(\frac{p_{XY}(x, y)}{p_X(x) p_Y(y)} \right) \quad (6)$$

where $p_X(x)$ and $p_Y(y)$ are the marginal probability distribution functions of X and Y respectively, and $p_{XY}(x, y)$ is the joint possibility supply role of X and Y .

Automatically, MI measures the data that X and Y segment: It calculates how much knowledge of one of these variables decreases uncertainty about the other. For sample, if X and Y are autonomous, then knowing X does not give any data near and evil versa, so their MI is nil. At the other risky, if X is a deterministic role of Y and Y is a deterministic role of X then all substantial occupied by X is collective with Y : important X panels the rate of Y and vice versa. As an outcome, in this situation the MI is the similar as the doubt controlled in Y (or X) unaided, specifically the information of Y (or X). Moreover, this MI is the same as the entropy of X and as the information of Y . A very special case of this is when X and Y are the similar chance flexible.

4.2 The Correlation Statistic Features Between NSCT Subband Coefficients

The MI of the coefficients is calculated as a quantitative evaluation of the dependencies to analyze the connection of the NSCT coefficients quantitatively. Based on the analysis of Sections 3.2 and 3.3, we mainly compute the following MI statistic features:

- (1) $MI(X, PX)$, where X denotes an NSCT coefficient, and PX denotes its parent in the next coarser subband.
- (2) $MI(X, CX)$, where CX denotes its cousins in the same scale and same spatial location but in different directional subbands.

In addition, the correlation between a coefficient and its cousins of adjacent direction is relatively stronger in all its relative coefficients. If we consider MI between all the relative coefficients, the correlation statistic features of NSCT subband coefficient must be redundant. In order to reduce the complexity and improve the operation efficiency of evaluation model, we only consider $MI(X, CX)$ between NSCT coefficients and their cousins of adjacent direction. In this paper, all pictures are disintegrated into two stages with the amount of commands 8 and 8 respectively. So the numbers of $MI(X, PX)$ and $MI(X, CX)$ that extracted from NSCT subband coefficients are 8 and 16 respectively. Fig. 6 depicts a natural undistorted image “rapids” as well as different warped variants from the LIVE IQA database, and in Fig. 7, we plot those MI statistic features of Fig. 6. Fig. 8 shows the MI statistic features of different distorted degree images for various distorted versions of natural undistorted image “rapids” respectively.



(a) rapids

(b) jp2k

(c) jpeg

Fig. 6. From the LIVE IQA database, there are natural undistorted picture “rapids” as well as numerous warped images.



Fig. 6. (Cont'd) From the LIVE IQA database, there are natural undistorted picture “rapids” as well as numerous warped images.

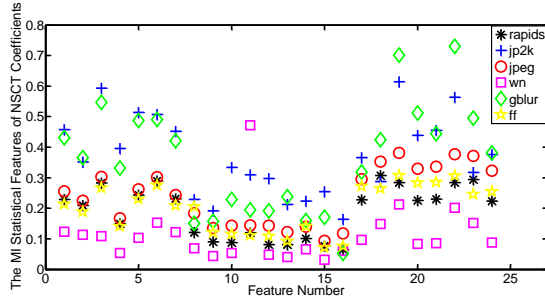


Fig. 7. The MI statistic features for “rapids” and its five distorted versions in Fig. 6.

From Fig. 7, we know that the MI statistic features between parent-child coefficients or relative coefficients can distinguish images of different distortion types. The main reasons are as follow: (1) the additive Gaussian noise that can enhanced the high frequency information of the image and generate pseudo-edge decreases the MI features; (2) the gaussian blur which can weaken the edge and texture of image increases the MI features; (3) “jpeg” that is based on DCT can eliminate much high occurrence indication from “rapids” and make the reference image produce blockiness; (4) Similar to “jpeg”, “jp2k” can remove a lot of high-frequency information to create a blur effect and “ff” is a combination of “jp2k” followed by packet-loss errors.

From each of Fig. 8, we can find that the MI statistic features values of different distorted degree images for the same distorted version are significantly different. In other words, whether it is a different type of distortion or varying degrees of distortion, the MI statistics features in NSCT domain can be clearly distinguished so we think that these features can be used to identify the type of distortion and predict the distortion-specific quality.

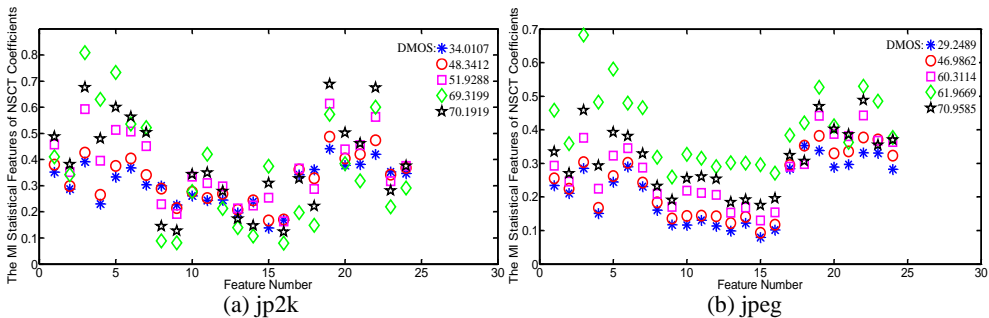


Fig. 8. (a)-(b) The MI statistic features of different distorted versions and different distorted degree images for natural undistorted image “rapids”.

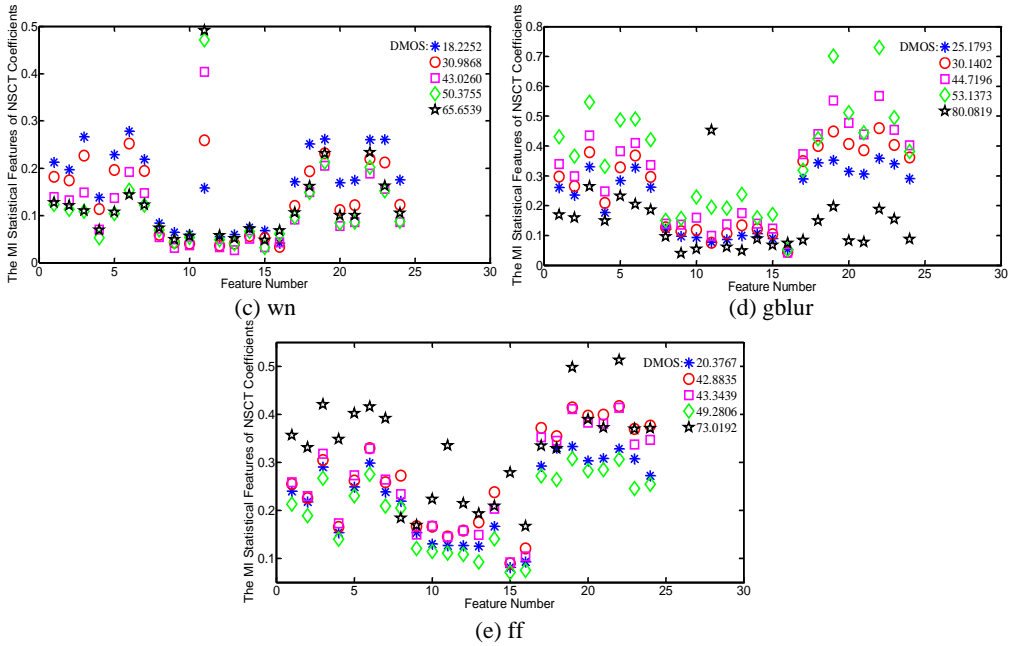


Fig. 8. (c)-(e) The MI statistic features of different distorted versions and different distorted degree images for natural undistorted image “rapids”.

4.3 The Structure Information Statistic Features of NSCT Subband Coefficients

As we all know, natural images are highly structured and neighboring image pixels are highly correlated with each other. Research has found that HVS is highly adapted to extract structural information from the visual scene, such as outline and texture information, and Neurons in the primary visual cortex are multiscale bandpass orientated filters with well-modeled localization that breakdown pictures into many visual channels. Surprisingly, some psychophysical research suggests that picture pattern recognition tasks may utilise the same set of visual channels. Moreover, the outline in the mid-frequency band is the most sensitive to HVS.

The NSCT which has fully shift-invariant is a multi-scale, local, multi-direction and overcomplete image representation. The low-frequency and high-frequency sub-images of an image decomposed by NSCT have the same size as the source image at each level and direction, and the high-frequency sub-images remain the basic outline of the original image. Moreover, the outline is the most important structure information of image and NSCT decomposition doesn't make the structure information of image loss. The structure features extracted from different frequency information using NSCT decomposition is more consistent with human visual characteristics. According to the above analysis, there are strong correlations between NSCT subband coefficients, especially parent-child coefficients and relative coefficients so we think that the structure information of those subband coefficients are similar and the similarity are changed when distortion occurs. And it can be used to forecast the sort of distortion that affects an image's perceived quality by quantifying these changes.

Each NSCT subband is compared with its parent and cousins using a windowed structural correlation [25] respectively. The structural correlation is computed as

$$s(X, Y) = \frac{\sigma_{XY} + C}{\sigma_X \sigma_Y + C} . \tag{7}$$

Where X and Y are two discrete non-negative signals that have been aligned with each other. σ_X^2, σ_Y^2 are the variance of X and Y respectively, and σ_{XY} is the covariance of them. C is a stabilising constant that eliminates instability as the denominator approaches zero, and its value is the same as in [25].

Based on the analysis of Sections 3.2 and 3.3, we mainly compute the following structure information statistic features:

- (1) $s(X, PX)$ where X denotes a NSCT coefficient, and PX denotes its parent in the next coarser subband.
- (2) $s(X, CX)$ where CX denotes its cousins in the same scale and same spatial location but in different directional subbands.

With the same to Section 4.2, all pictures are disintegrated into two stages with the amount of instructions 8 and 8 in this paper respectively and we also only consider $s(X, CX)$ between NSCT coefficients and their cousins of adjacent direction so the numbers of $s(X, PX)$ and $s(X, CX)$ that extracted from NSCT subband coefficients are 8 and 16 respectively. Fig. 9 shows the structure information statistic features of Fig. 6. Fig. 10 show the structure information statistic features of different distorted degree images for various distorted versions of natural undistorted image “rapids” from LIVE IQA database respectively.

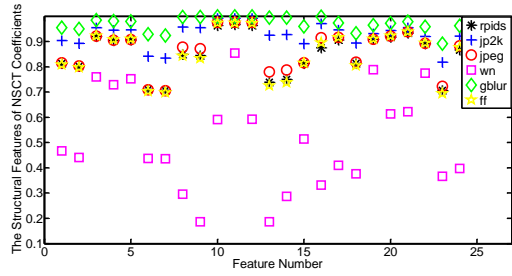


Fig. 9. The structure information statistic features for “rapids” and its five distorted versions in Fig. 6.

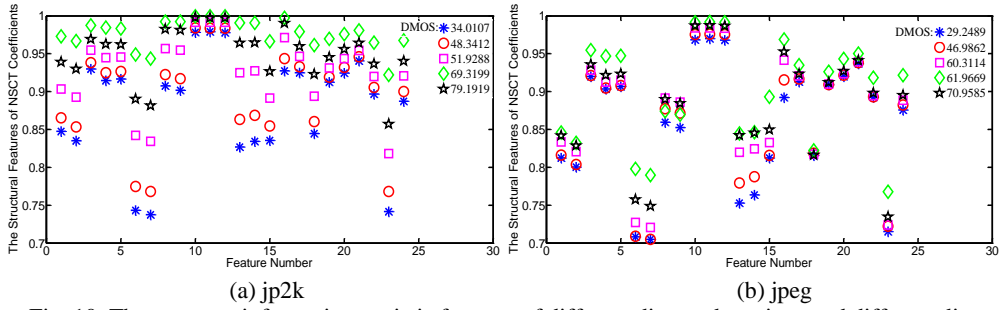


Fig. 10. The structure information statistic features of different distorted versions and different distorted degree images for natural undistorted image “rapids”.

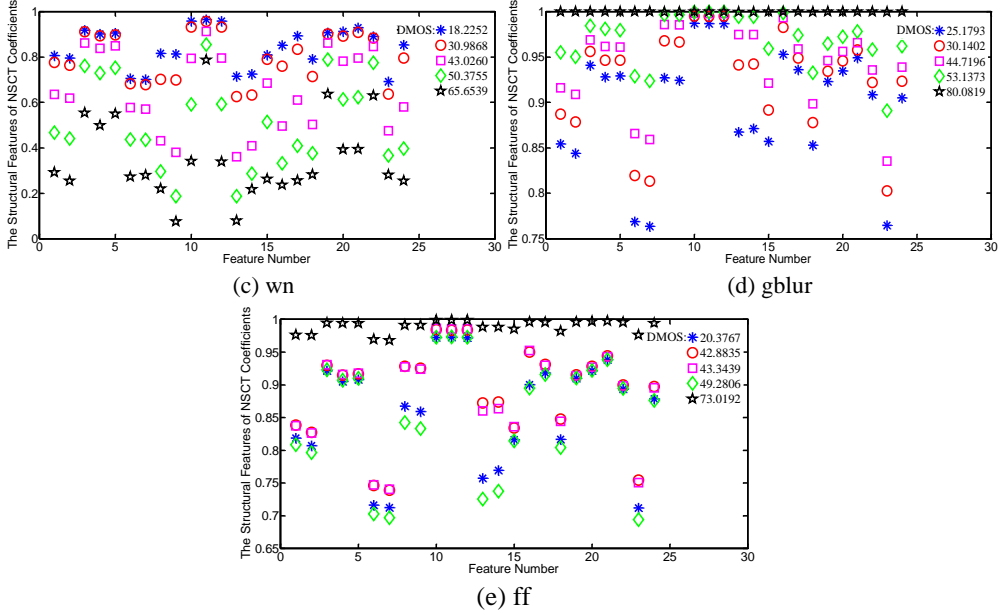


Fig. 10. The structure information statistic features of different distorted versions and different distorted degree images for natural undistorted image “rapids”

From Figs. 9 and 10, we can get the similar results as Figs. 7 and 8 respectively. In short, the structure information statistic features between parent-child coefficients or relative coefficients can not only distinguish images of different distortion types, also can clearly distinguish images of different distortion degree. So those structure information statistic features can be used to recognition image distortion type and evaluate the image objective quality.

4.4 The Statistics Features in NSCT Domain and Spatial Domain

The MI statistical features and the structure information statistical features of NSCT subband coefficients mainly reflect the correlation between those coefficients, and the statistical features of MSCN coefficients can reflect the luminance contrast and the characteristics of direction neighborhood, so we think that it can more comprehensive to evaluate the image quality by combining with those statistic features. We extract the statistics features in NSCT domain and spatial domain listed in Table 3. A total of 84 features are used to perform distortion-specific quality assessment.

In Fig. 11, we exhibit the SROCC among each of these characteristics and human DMOS spanning all distorted categories in the LIVE IQA database and all distorted images to show how each of these features collects quality information and is influenced in the presence of distortion. Furthermore, no training is provided here. Fig. 11 shows that, for the most part, the statistical features of MSCN coefficients have better connection with social awareness than the MI statistical features and the structure information statistic features of NSCT coefficients. But as described previously, the MI statistics features and the

structure information statistic features in NSCT domain have relatively better discrimination. Therefore, by combining with the statistical features of spatial domain and NSCT domain, it can not only effectively evaluate the quality of image, can also effectively identify their distortion types.

Table 3. Feature extraction description.

Features	Feature Description	Computing Method
$f_1 - f_8$	Correlation between NSCT relative coefficients in 1 st scale	Compute MI between NSCT relative coefficients in 1 st scale
$f_9 - f_{16}$	Correlation between NSCT relative coefficients in 2 nd scale	Compute MI between NSCT relative coefficients in 2 nd scale
$f_{17} - f_{24}$	Correlation between NSCT coefficients and its parent coefficients	Compute MI between NSCT coefficients and its parent coefficients
$f_{25} - f_{32}$	Structure information between NSCT relative coefficients in 1 st scale	Compute windowed structural correlation between NSCT relative coefficients in 1 st scale
$f_{33} - f_{40}$	Structure information between NSCT relative coefficients in 2 nd scale	Compute windowed structural correlation between NSCT relative coefficients in 2 nd scale
$f_{41} - f_{48}$	Structure information between NSCT coefficients and its parent coefficients	Compute windowed structural correlation between NSCT coefficients and its parent coefficients
$f_{49} - f_{50}$	Shape and variance in 1 st scale	Fit GGD to MSCN coefficients
$f_{51} - f_{66}$	Figure, unkind, left and right change in 1 st scale	Fit AGGD to neighboring MSCN constants
$f_{67} - f_{68}$	Shape and variance in 2 nd scale	Fit GGD to MSCN constants
$f_{69} - f_{84}$	Figure, unkind, left and right change in 2 nd scale	Fit AGGD to neighboring MSCN constants

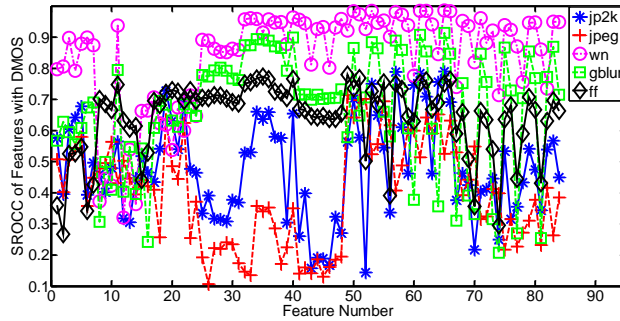


Fig. 11. SROCC between features and DMOS for different distortions.

4.5 Prediction Model

Given the NSCT and MSCN coefficients feature vectors which contain 84 features, TDSDQA needs a plotting since the feature space measured here to image quality scores to assess image quality. The support vector machine (SVM) is a learning methodology

based on Vapnik Chervonenkis (VC) theory and able to deal with classification and regression problems. The theory is a type of computational learning theory that tries to explain how people learn from a statistical standpoint. Nonlinear SVR is solved with a kernel function, which leads to high accuracy and optimal generalization performance, but at the same time a high computational effort. Lee *et al.* [39] suggested an epsilon-SVR formulation in which they just had to solve a system of linear equations iteratively rather than a convex quadratic programme or a linear programme, as in a traditional epsilon-SVR. Furthermore, they suggest a kernel reduction, although the decreased vectors in the kernel are just a portion of the training data. In addition, SVR has previously been applied to IQA problem and is usually well-known for presence intelligent to holder high dimensional information so we select the epsilon-SVR to construct the mapping.

We utilize the Libsvm-3.18 package [26] developed by Dr. Chih-Jen Lin to build the regression models, which is an integrated software for support vector classification, (C-SVC, nu-SVC), regression (epsilon-SVR, nu-SVR) and distribution estimation (one-class SVM). The f and their distorted versions and the testing subsets contain 20%, and no overlap between train and test content occurs. We repeat to run the random train-test procedure 1000 times, and the median of the performance across these 1000 iterations is reported. Besides, to establish a fair comparison, we run an identical 20% test set selection 1000 times to obtain the FR-median IQA's performance indices approaches which do not need training.

In order to access performance of the above-mentioned IQA methods, we used the SROCC which serves as a measure of the prediction monotonicity and PLCC which serves as a measure of the prediction accuracy among the projected score from the procedure and DMOS. Tables 4 and 5 report the average SROCC and LCC outcomes verified on LIVING IAQ record respectively. From them, we observed that TDSDQA slightly outperforms the FR-IQA methods, as well as the state-of-the-art general-purpose NR-IQA methods algorithms considered here. For most of distortion types, it also outperforms the above-mentioned IQA methods, especially jp2k and ff.

Table 4. Median SROCC across 1000 train-test combinations on live image database.

Type	Algorithm	jp2k	jpeg	gblur	wn	ff	all
<i>FF-IQA</i>	PSNR	0.8646	0.8831	0.9410	0.7515	0.8736	0.8636
	SSIM	0.9389	0.9466	0.9635	0.9046	0.9393	0.9129
	MS-SSIM	0.9627	0.9785	0.9773	0.9542	0.9386	0.9535
	BRISUE [11]	0.9139	0.9647	0.9786	0.9511	0.8768	0.9395
	SSEQ [12]	0.9420	0.9510	0.9784	0.9483	0.9035	0.9348
	MIQA [13]	0.9408	0.9259	0.9828	0.9572	0.8800	0.9333
	BLIINDS-II [14]	0.9323	0.9331	0.9463	0.8912	0.8519	0.9124
	<i>NR-IQA</i>	DIIVINE [15]	0.9123	0.9208	0.9818	0.9373	0.8694
	C-DIIVINE [16]	0.9302	0.9444	0.9760	0.9386	0.9110	0.9444
	CurveletQA [17]	0.9367	0.9117	0.9876	0.9650	0.9005	0.9303
	SHANIA [18]	0.8611	0.8918	0.9582	0.9674	0.9169	0.9033
	TDSDQA	0.9395	0.9126	0.9749	0.9645	0.9249	0.9507

Table 5. Median PLCC across 1000 train-test combinations on live image database.

Type	Algorithm	jp2k	jpeg	gblur	wn	ff	all
<i>FF-IQA</i>	PSNR	0.8762	0.9029	0.9173	0.7801	0.8795	0.8592
	SSIM	0.9405	0.9462	0.9824	0.9004	0.9514	0.9066
	MS-SSIM	0.9746	0.9793	0.9883	0.9645	0.9488	0.9511
<i>NR-IQA</i>	BRISUE [11]	0.9229	0.9734	0.9851	0.9506	0.9030	0.9424
	SSEQ [12]	0.9464	0.9702	0.9806	0.9607	0.9198	0.9383
	MIQA [13]	0.9405	0.9276	0.9802	0.9515	0.8917	0.9232
	BLIINDS-II [14]	0.9386	0.9426	0.9635	0.8994	0.8790	0.9164
	DIIVINE [15]	0.9233	0.9347	0.9867	0.9370	0.8916	0.9270
	C-DIIVINE [16]	0.9429	0.9593	0.9844	0.9412	0.9345	0.9474
	CurveletQA [17]	0.9465	0.9280	0.9887	0.9694	0.9186	0.9328
	SHANIA [18]	0.9135	0.9380	0.9731	0.9790	0.9413	0.9412
	TSDQA	0.9548	0.9472	0.9880	0.9712	0.9476	0.9519

4.6 Database Independence

In order to show if the IQA database on which TSDQA is trained has an impact on its performance. We utilised the LIVING IQA record as a whole to train the TSDQA and the TID2008 database to test it respectively. In addition, the LIVING IQA record contains 5 distortion types and its images are all natural image. In order to be common with the LIVE IQA folder, so we only used the 24 natural images and their 4 distortion categories (jp2k, jpeg, wn and gblur) on the TID2008 database to test. The results of TSDQA and four NR-IQA methods are shown in Table 6 shows that, despite the lower performance, distorted pictures are formed in various ways across LIVE and TID2008, TSDQA achieves healthy in standings of connection with social awareness of worth and is superior to the NR-IQA approaches considered here.

Table 6. Srocc on tid2008 image database.

Type	Algorithm	jp2k	jpeg	wn	gblur	all
<i>FF-IQA</i>	PSNR	0.8250	0.8760	0.9230	0.9342	0.8700
	SSIM	0.9603	0.9354	0.8168	0.9544	0.9016
<i>NR-IQA</i>	BRISUE [11]	0.8320	0.9240	0.8290	0.8810	0.8960
	BLIINDS-II [14]	0.9147	0.8889	0.6956	0.8572	0.8542
	DIIVINE [15]	0.9240	0.8660	0.8510	0.8620	0.8890
	C-DIIVINE [16]	0.9370	0.9240	0.8090	0.9000	0.9210
	CurveletQA [17]	0.5499	0.8647	0.8589	0.8827	0.8672
	TSDQA	0.9259	0.9048	0.8786	0.9123	0.9233

4.7 Classification Performance Analysis

For each of the distortions in the LIVE IQA database, as well as across all distortions, we computed the median classification accuracies of 1000 train-test trails, to show that TSDQA characteristics may be employed for diverse distortion detection. Table 7 reports the results. Further, to visualize the mutual confusion relationship of each distortion type. A mean confusion matrix is plotted in Fig. 12 with the genuine distortion class on the

vertical axis and the anticipated distortion class on the horizontal axis. The real numbers are the mean confusion % throughout the 1000 train-test trails, and the total of each row in this matrix is 1.

Table 7. Median classification accuracy crossways 1000 train-test trials on living image record.

Algorithm	jp2k	jpeg	wn	gblur	ff	all
<i>BRISUE</i> [11]	82.9%	88.9%	100%	96.7%	83.3%	88.6%
<i>SSEQ</i> [12]	61.76%	89.56%	100%	70%	46.67%	73.29%
<i>MIQA</i> [13]	73.53%	85.29%	100%	83.33%	60%	79.12%
<i>DIIVINE</i> [15]	80%	81.1%	100%	90%	73.33%	83.75%
<i>C-DIIVINE</i> [16]	88.9%	91.70%	100%	93.30%	73.30%	89.40%
<i>CurveletQA</i> [17]	71.43%	78.95%	100%	80%	46.67%	75%
<i>TSDQA</i>	94.12%	97.14%	100%	96.55%	89.66%	94.23%

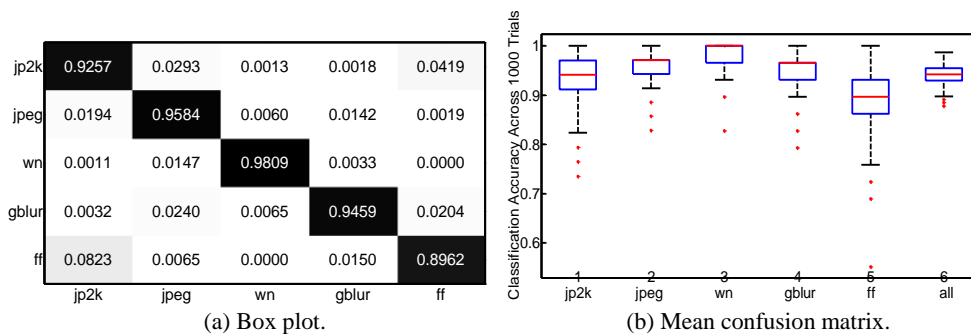


Fig. 12. Box plot and unkind mistake medium for alteration classifier crossways 1000 sleeper trial hearings.

Table 7 indicates that the median classification accuracy of TSDQA obviously outperforms the present stage-of-the-painting all-purpose NR-IQA methods. Because ff distortion is a mix of jp2k compression followed by packet-loss problems, Fig. 12 shows that jp2k and ff are easily misunderstood. Jpeg and jp2k are similar in that they both have blur, which increases the MI statistical properties. Gblur and wn, on the other hand, are difficult to mix up with other distortion kinds. The main reason is that wn can increase the high-frequency components and reduce the correlation between NSCT subband coefficients. By contrast, not only can blur increase the correlation between NSCT subband coefficients, but also its level is more evident than other distortion types.

4.8 Time Complexity Analysis

The time complexity is also an important performance to evaluate IQA algorithms. Generally, the feature extraction in IQA models can need to consume much higher time than prediction computed with SVR. The feature extraction of TSDQA can be mainly divided into four steps: (1) leading the NSCT decomposition on an image; (2) extracting MI statistics features from NSCT coefficients; (3) extracting the structure information

statistic features from NSCT coefficients; and (4) extracting NSS features from MSCN coefficients. We examined the proportional percentage of time it took to calculate each of the four feature types on a 720x1280 picture to assess their temporal complexity. The results are shown in Table 8.

In addition, to see how TDSDQA stacks up against the other NR-IQA techniques in terms of total computational complexity which code is publicly available and avoid the influence of other factors, we used all the images with resolution 720x1280 from the LIVING Multiply Distorted IQA record and calculated the average run time. The test was carried out on a Lenovo supercomputer with a square essential CPU, 3.2GHz, and 4 GB RAM, running Windows 7 Pro 32-bit. Table IX displays the outcomes. As the Table 9 demonstrates, the TDSDQA is better than the BLIINDS-II index and the DIIVINE index, but inferior to the CurveletQA index, SSEQ index and the BRISUE index.

Table 8. Percentage of time consumed by each of step in TDSDQA.

Step	Percentage of time (%)
<i>NSCT decomposition</i>	29.00
<i>extracting MI statistics features from NSCT coefficients</i>	38.56
<i>extracting structure features from NSCT coefficients</i>	29.39
<i>extracting NSS features from MSCN coefficients</i>	3.05

Table 9. A comparison of the runtime consumed for five NR-IQA algorithms.

NR-IQA Algorithm	Time (seconds)
<i>BRISUE</i> [11]	0.388
<i>SSEQ</i> [12]	5.22
<i>BLIINDS-II</i> [14]	57.06
<i>DIIVINE</i> [15]	200.03
<i>CurveletQA</i> [17]	4.21
<i>TDSDQA</i>	14.095

4.9 Robustness Analysis

Because the TDSDQA approach necessitates a calibration procedure for the regression module, the different proportion of the training and testing image subsets may affect the evaluation and recognition of corresponding model respectively. In order to analyze how much it affects the evaluation model and recognition model, we adopt the similar method with Sections 6.1 and 6.3 to design six experiments respectively. The results of evaluation model and recognition model are shown in Tables 10 and 11 respectively.

As the Tables 4, 5 and 10 demonstrate, with the reduction of the training images, the SROCC and PLCC between the evaluation scores of TDSDQA and DMOS decrease in the whole and each distortion versions. But the extent of reduction is not obvious, and the corresponding SROCC and PLCC in the whole distortion versions are still up to 0.9 while twenty percent images of the LIVING IQA record are secondhand to train. As a consequence, the TDSDQA evaluation findings are highly correlated with human image quality assessments. To put it another way, the assessment model is both effective and reliable.

Table 10. Average SROCC and PLCC across 1000 train-test trials under different proportion of training subsets and test subsets on live image database.

training subsets and testing subsets		jp2k	jpeg	wn	gblur	ff	all
70% and 30%	<i>SROCC</i>	0.9423	0.9148	0.9758	0.9629	0.9232	0.9495
	<i>PLCC</i>	0.9520	0.9446	0.9866	0.9648	0.9407	0.9498
60% and 40%	<i>SROCC</i>	0.9403	0.9100	0.9754	0.9603	0.9194	0.9457
	<i>PLCC</i>	0.9486	0.9413	0.9847	0.9583	0.9334	0.9455
50% and 50%	<i>SROCC</i>	0.9379	0.9050	0.9736	0.9555	0.9152	0.9410
	<i>PLCC</i>	0.9452	0.9370	0.9832	0.9528	0.9269	0.9402
40% and 60%	<i>SROCC</i>	0.9331	0.9007	0.9705	0.9486	0.9060	0.9343
	<i>PLCC</i>	0.9402	0.9327	0.9797	0.9445	0.9168	0.9334
30% and 70%	<i>SROCC</i>	0.9259	0.8909	0.9647	0.9345	0.8945	0.9239
	<i>PLCC</i>	0.9321	0.9256	0.9750	0.9317	0.9027	0.9227
20% and 80%	<i>SROCC</i>	0.9222	0.8865	0.9649	0.9232	0.8612	0.9112
	<i>PLCC</i>	0.9283	0.9204	0.9748	0.9200	0.8668	0.9092

Table 11. Average arrangement accurateness crossways 1000 sleeper hearings under different proportion of training subsets and test subsets on live image database.

training subsets and testing subsets	jp2k	jpeg	wn	gblur	ff	all
70% and 30%	92%	96.15%	97.67%	95.35%	88.37%	93.94%
60% and 40%	91.04%	95.71%	98.28%	94.83%	87.93%	93.25%
50% and 50%	90.48%	95.40%	98.61%	93.06%	84.72%	92.38%
40% and 60%	90.10%	94.29%	98.85%	91.95%	82.76%	91.22%
30% and 70%	88.14%	92.62%	98.02%	91.09%	78.22%	89.32%
20% and 80%	85.19%	89.29%	98.28%	87.93%	71.55%	86.20%

Tables 7 and 11 show that the classification accuracies of TDSDQA decrease slightly in the whole and each distortion versions with the reduction of training images. But it still maintains higher classification accuracy. Even only forty percent images for training in the LIVE IQA database, the classification accuracy of TDSDQA is still up to 91.22%. It is still higher compared to other states NR-IQA algorithms that are state-of-the-art, such as BRISUE [11], SSEQ [12], MIQA [13], DIIVINE [15], C-DIIVINE [16] and CurveletQA [17] *etc.* In short, the recognition model also has good robustness.

5. CONCLUSIONS

In the realm of image and video processing, as well as many practical settings, quality evaluation for digital visual signals is one of the most fundamental and difficult topics, such as process evaluation, implementation, optimization, testing and monitoring. It can build a bridge between the assessment of quality as experienced by the end-user and the quality of service parameters that are usually deployed to quantify service integrity. Especially NR-IQA has been a topic of intense research over the last decade and continued to grow at an astounding rate.

In this research, we provide TDSDQA, a general-purpose NR-IQA method based on statistical characterization in both the NSCT and geographical domains. We studied the variation of statistics features extracted by this paper along with the distortion types and distortion level respectively, and found that the MI statistics features and the structure in-

formation statistic features between NSCT subband coefficients have relatively better discrimination. The spatial domain characteristics, on the other hand, are a beneficial, performance-enhancing supplement to the MI statistical features and the structure information statistic features in NSCT domain. Experimental results also show that TSDQA predict image qualities in a meaningful agreement with the human judgment and is competitive with top-performing NR-IQA approaches. Feature work will mainly involve increasing the operating efficiency of TSDQA and achieving close to real time. Besides, MI statistics features and the structure information statistic features in NSCT domain can also be considered to classify the distortion images.

ACKNOWLEDGEMENT

This work was supported by “the Fundamental Research Funds for the Provincial Universities,” Zhejiang Institute of Economics and Trade (Grant Number: 19TQ23).

REFERENCES

1. H. R. Sheikh, M. F. Sabir, and A. C. Bovik, “A statistical evaluation of recent full reference image quality assessment algorithms,” *IEEE Transactions on Image Process*, Vol. 15, 2006, pp. 3440-3451.
2. H. R. Sheikh, A. C. Bovik, and L. Cormack, “No-reference quality assessment using natural scene statistics: JPEG2000,” *IEEE Transactions on Image Process*, Vol. 14, 2005, pp. 1918-1927.
3. J. Wu, M. Zhang, L. Li, W. Dong, G. Shi, and W. Lin, “No-reference image quality assessment with visual pattern degradation,” *Information Sciences*, Vol. 504, 2019, pp. 487-500.
4. X. Yang, Q. Sun, and T. Wang, “No-reference image quality assessment based on sparse representation,” *Neural Computing and Applications*, Vol. 31, 2019, pp. 6643-6658.
5. I. F. Nizami, M. Majid, and K. Khurshid, “New feature selection algorithms for no-reference image quality assessment,” *Applied Intelligence*, Vol. 48, 2018, pp. 3482-3501.
6. Y. Zhou, L. Li, S. Wang, J. Wu, Y. Fang, and X. Gao, “No-reference quality assessment for view synthesis using DoG-based edge statistics and texture naturalness,” *IEEE Transactions on Image Process*, Vol. 28, 2019, pp. 4566-4579.
7. L. S. Chow and H. Rajagopal, “Modified-BRISQUE as no reference image quality assessment for structural MR images,” *Magnetic Resonance Imaging*, Vol. 43, 2017, pp. 64-75.
8. J. Wu, Z. Xia, H. Li, K. Sun, K. Gu, and H. Lu, “No-reference image quality assessment with center-surround based natural scene statistics,” *Multimedia Tools and Applications*, Vol. 77, 2018, pp. 20731-20751.
9. T. Brandao and M. P. Queluz, “No-reference image quality assessment based on DCT-domain statistics,” *Signal Process*, Vol. 88, 2008, pp. 822-833.
10. M. Oszust, “No-reference image quality assessment using image statistics and robust feature descriptors,” *IEEE Signal Processing Letters*, Vol. 24, 2017, pp. 1656-1660.

11. A. Mittal, A. K. Moorthy, and A. C. Bovik, "No-reference image quality assessment in the spatial domain," *IEEE Transactions on Image Process*, Vol. 21, 2012, pp. 4695-4708.
12. L. X. Liu, B. Liu, H. Huang, and A. C. Bovik, "No-reference image quality assessment based on spatial and spectral entropies," *Signal Processing: Image Communication*, Vol. 29, 2014, pp. 856-863.
13. H. P. Dong and L. X. Liu, "No-reference image quality assessment in mutual information domain," *Journal of Image and Graphics*, Vol. 19, 2014, pp. 484-492.
14. M. A. Saad, A. C. Bovik, and C. Charrier, "Blind image quality assessment: A natural scene statistics approach in the DCT domain," *IEEE Transactions on Image Processing*, Vol. 21, 2012, pp. 3339-3352.
15. A. K. Moorthy and A. C. Bovik, "Blind image quality assessment: From natural scene statistics to perceptual quality," *IEEE Transactions on Image Processing*, Vol. 20, 2011, pp. 3350-3364.
16. Y. Zhang, A. K. Moorthy, D. M. Chandler, and A. C. Bovik, "C-DIIVINE: No-reference image quality assessment based on local magnitude and phase statistics of natural scenes," *Signal Processing: Image Communication*, Vol. 29, 2014, pp. 725-747.
17. L. X. Liu, H. P. Dong, and H. Huang, "No-reference image quality assessment in curvelet domain," *Signal Processing: Image Communication*, Vol. 29, 2014, pp. 494-505.
18. Y. M. Li, L. M. Po, X. Y. Xu, and L. Feng, "No-reference image quality assessment using statistical characterization in the shearlet domain," *Signal Processing: Image Communication*, Vol. 29, 2014, pp. 748-759.
19. J. Shen, Q. Li, and G. Erlebacher, "Hybrid No-reference natural image quality assessment of noisy, blurry, JPEG2000, and JPEG images," *IEEE Transactions on Image Processing*, Vol. 20, 2011, pp. 2089-2098.
20. H. R. Sheikh, Z. Wang, L. Cormack, and A. C. Bovik, "LIVE image quality assessment database release 2," <http://live.ece.utexas.edu/research/quality>.
21. N. Ponomarenko, V. Lukin, A. Zelensky, K. Egiazarian, M. Carli, and F. Battisti, "TID2008 – A database for evaluation of full-reference visual quality assessment metrics," *Advances of Modern Radioelectronics*, Vol. 10, 2009, pp. 30-45.
22. A. S. Alghamdi, K. Polat, A. Alghoson, A. A. Alshdadi, and A. A. El-Latif, "Gaussian process regression (GPR) based non-invasive continuous blood pressure prediction method from cuff oscillometric signals," *Applied Acoustics*, Vol. 164, 2020, p. 107256.
23. J. Gao, H. Wang, and H. Shen, "Smartly handling renewable energy instability in supporting a cloud datacenter," in *Proceedings of IEEE International Parallel and Distributed Processing Symposium*, 2020, pp. 769-778.
24. P. Mangalraj, V. Sivakumar, S. Karthick, V. Haribaabu, S. Ramraj, and D. J. Samuel, "A review of multi-resolution analysis (MRA) and multi-geometric analysis (MGA) tools used in the fusion of remote sensing images," *Circuits, Systems, and Signal Processing*, Vol. 39, 2019, pp. 3145-3172.
25. D. L. Ruderman, "The statistics of natural images," *Network: Computation in Neural Systems*, Vol. 5, 1994, pp. 517-548.
26. E. C. Larson and D. M. Chandler, "Categorical subjective image quality CSIQ database," 2009, <http://vision.okstate.edu/csiq/>.

27. A. L. D. Cunha, J. P. Zhou, and M. N. Do, "The nonsubsampling contourlet transform: theory, design, and applications," *IEEE Transactions on Image Processing*, Vol. 15, 2006, pp. 3089-3101.
28. Z. Wang, A. C. Bovik, H. R. Sheikh, and E. P. Simoncelli, "Image quality assessment: From error measurement to structural similarity," *IEEE Transactions on Image Processing*, Vol. 13, 2004, pp. 600-612.
29. C. C. Chang and C. J. Lin, "LIBSVM: a library for support vector machines," *ACM Transactions on Intelligent Systems and Technology*, Vol. 2, 2011, pp. 1-27.



Guiying Zhu was born in Cangzhou, Hebei, P.R. China, in 1981. She received the Master degree from Zhejiang Sci-Tech University, P.R. China. Now, she works in School of Department of Applied Engineering, Zhejiang Institute of Economics and Trade. Her research interests include automotive electronic technology and computer image processing. E-mail: zhuguiyingdn@163.com